SNR simulations for Genesis VT observations

SNR simulations for Genesis VT observations

H. Sert, M. Schartner, A. Özyıldırım, R. Haas, Ö. Karatekin

Abstract The signal-to-noise ratio (SNR) of Genesis signals on a baseline between two VLBI Global Observing System (VGOS) telescopes is a critical factor influencing data quality and delay estimation. The SNR on a given baseline depends on various factors, including the received power flux density (PFD) at each station. In traditional VLBI observations of quasars at cosmological distances, the incoming radio signals arrive at the ground stations with approximately equal power, resulting in a uniform PFD across identical telescopes. However, in the case of a VLBI transmitter (VT) onboard an Earth-orbiting satellite, the received signal power varies across different ground stations due to the dynamic geometrical configurations between the satellite and each station. In this study, we conduct simulations over a one-day period to compute the SNR for different baselines, considering various antenna gains for Genesis Band A (3100–3300 MHz) signals.

Keywords VLBI, transmitter, SNR

1 Introduction

The uncertainty of Very Long Baseline Interferometry (VLBI) group delay measurements is intrinsically linked to the signal-to-noise ratio (SNR) of the observation, as demonstrated by Whitney (1974):

$$\sigma_\tau = \frac{1}{2\pi\,\mathrm{SNR}\,\Delta\nu_{\mathrm{RMS}}} \tag{1}$$

Here, σ_τ represents the uncertainty in the group delay, and $\Delta\nu_{\mathrm{RMS}}$ denotes the effective bandwidth (i.e., the root-mean-square of the spanned bandwidth) of the receiving system. The effective bandwidth accounts for the distribution of observing frequencies across the system and is computed as

$$\Delta\nu_{\mathrm{RMS}} = \sqrt{\frac{1}{n}\sum_{i=1}^{n}(\nu_i - \bar{\nu})^2}, \tag{2}$$

where ν_i is the frequency of the i-th channel, $\bar{\nu}$ is the mean frequency, and n is the total number of channels. The effective bandwidth $\Delta\nu_{\mathrm{RMS}}$ is crucial, as a wider bandwidth reduces the group delay uncertainty by improving the frequency resolution.

The SNR measures the strength of the observed signal relative to the noise level. For quasar observations, the theoretical SNR is calculated as

$$\mathrm{SNR} = \eta\,\frac{S}{\sqrt{\mathrm{SEFD}_1 \cdot \mathrm{SEFD}_2}} \cdot \sqrt{Nt}, \tag{3}$$

where SEFD_i is the *system equivalent flux density* for station i, η is the correlation efficiency factor — typically between 0.5 and 0.7 (Jaradat et al., 2021) —, t is the scan length (or integration time) of the observation, and S is the correlated power flux density (PFD) of the observed radio source, and N is the total data rate, taken as 2048 Mbit/s (Niell et al., 2018). For VLBI quasar observations, the typical source flux density is assumed to be $S \equiv 1$ Jy $= 1 \cdot 10^{-26}$ W Hz^{-1} m^{-2} (Nothnagel, 2021).

Hakan Sert[1,2] · Matthias Schartner[3] · Alime Özyıldırım[1] · Rüdiger Haas[4] · Özgür Karatekin[1]
(1) Royal Observatory of Belgium
(2) Université catholique de Louvain, Earth and Life Institute
(3) ETH Zurich, Institute of Geodesy and Photogrammetry
(4) Chalmers University of Technology, Onsala Space Observatory, Space, Earth and Environment

The SNR equation underscores the interplay between the characteristics of the radio source, the performance of the receiving antennas, and the observation parameters. Higher SNR values can be achieved through increased PFD, improved antenna efficiency, lower system noise temperatures, larger bandwidth, or longer integration times. These factors collectively contribute to reducing the uncertainty in group delay measurements, thereby enhancing the precision of VLBI observations. While the actual SNR is calculated during fringe fitting, the SNR equation can provide valuable insight into identifying areas where the system and observation layout can be optimized during the scheduling process to achieve better results (Schartner et al., 2019).

Assuming a single S, for both stations does not hold for satellite VLBI transmitter (VT) observations, as the Free Space Path Loss (FSPL) (and other possible losses) are unequal due to the varying distances between the satellite and the observing stations, which significantly affect the received signal strength. In the case of VLBI VT observations, the SNR for a baseline can be derived by combining the individual SNR values from both stations. This requires modifying the flux density term S in Eq. 3, using the relation of

$$S = \sqrt{S_1 \cdot S_2}. \tag{4}$$

This approach accounts for the unequal PFD values received at the two stations due to the different distances between the (near-field) satellite and the observing stations. Thus, SNR equation for VT observations can be given as

$$\mathrm{SNR} = \eta \frac{\sqrt{S_1 \cdot S_2}}{\sqrt{\mathrm{SEFD}_1 \cdot \mathrm{SEFD}_2}} \cdot \sqrt{Nt}, \tag{5}$$

To compute the SNR of VT observations, it is therefore important to take into account the PFD for individual VLBI ground stations. This requires considerations of gains/losses for given satellite-station configurations as well as receiver/transmitter specifications.

2 Received power flux density at the ground stations

The PFD at a ground station i from a radio source is determined by the received power (P_r) and the bandwidth of the signal ($\Delta\nu$), i.e.

$$S_i = \frac{P_r}{A_e \Delta\nu}, \tag{6}$$

where A_e is the effective area of the telescope defined as the physical aperture area multiplied by an efficiency factor, k, typically ranging from 0.4 to 0.6 (Jaradat et al., 2021) and set to 0.5 in this study. Given a desired power flux density S_i at the VLBI telescope, the received power is hence determined as

$$P_r[W] = 10^{-26} \cdot S_i\,[\mathrm{Jy}] \cdot \Delta\nu\,[\mathrm{Hz}] \cdot A_e\,[\mathrm{m}^2], \tag{7}$$

where S_i represents the power flux density in units of Jansky. Note that the terms with squared brackets represent the units for each parameter.

The received power on a ground station can be obtained by considering all gains and losses for the given transmitter power, P_t. The *Friis transmission equation* (Stutzman & Thiele, 2012) provides a relationship considering VT and telescope gains and Free Space Path Loss ($\mathrm{FSPL} = (4\pi R/\lambda)^2$) for given VT power P_t in linear form

$$\frac{P_r}{P_t} = G_t G_r \Big(\frac{\lambda}{4\pi R}\Big)^2, \tag{8}$$

where G_t and G_r are the transmitter and receiving telescope gains, λ is the signal wavelength, and R is the distance between the VT and the ground station. Telescope gain is given as (Jaradat et al., 2021)

$$G_r = k(\pi d/\lambda)^2 \tag{9}$$

where d is the diameter of telescope which is assumed to be 13.2 m in this study, and k is the aperture efficiency. Substituting the expression for P_r in Eq. 7 into Eq. 8, the required transmitter power in watt per hertz for a given bandwidth can be written as

$$\frac{P_t[W]}{\Delta\nu[Hz]} = \frac{\mathrm{FSPL}}{G_t G_r} S_i \cdot 10^{-26} \cdot A_e. \tag{10}$$

Once P_t is determined, the received flux density at the telescope for different configurations can be found by rearranging Eq. 8. For a fixed P_t, the PFD at the telescope i is given by

$$S_i[\mathrm{Jy}] = \frac{1}{10^{-26}} \frac{P_t}{A_e \Delta\nu} G_t G_r \Big(\frac{\lambda}{4\pi R}\Big)^2. \tag{11}$$

2.1 VT Antenna Gain

Antenna gain measures how effectively an antenna directs power in a specific direction, compared to an isotropic antenna. The antenna radiation pattern describes how power varies with direction. The solid angle, Ω, of the main lobe is given by the product of the Half Power Beam Width (HPBW) angles in two principal planes ($\Omega = \theta_{HPBW} \cdot \phi_{HPBW}$) and the directivity D of an antenna is defined as the ratio of the solid angle of an isotropic antenna to that of the directional antenna:

$$D = 4\pi/\Omega \tag{12}$$

Considering that the Earth's field-of-view from the Genesis altitude of 6000 km is approximately 62° in both planes, the required HPBW to fully cover this region is also $\theta \approx \phi \approx 62^\circ$. According to Eq. 12, this corresponds to a directivity value of approximately $D = 10$, indicating that the signal strength at boresight is about 10 times higher than that of an isotropic antenna and decreases with increasing boresight angle. Any off-axis deviation can be accounted for by the radiation pattern factor, f_{arp}, which represents how the signal power varies as a function of the boresight angle. Then the directivity for a given angular position can be obtained by

$$D_i = D \cdot f_{arp}(\theta, \phi), \tag{13}$$

which takes into account how the signal power is directed for a given boresight angle. Finally, the antenna gain G_t, considering directivity and efficiency, is given by

$$G_t = \mu D_i, \tag{14}$$

where μ is the efficiency factor of the VT antenna, set to 0.7 in this work.

We consider directional radiation patterns modeled as $\cos^n(\theta)$, where the exponent n controls the rate of signal attenuation with boresight angle. Specifically, we use patterns that produce signal drops of $0\,\mathrm{dBi}$ (isotropic), $3\,\mathrm{dBi}$, $6\,\mathrm{dBi}$, and $9\,\mathrm{dBi}$ at the edge of Earth's field of view, denoted as $P0$, $P3$, $P6$, and $P9$, respectively.

3 Simulations and results

We simulate a one-day orbit of the planned Genesis satellite (Delva et al., 2023), which will operate in a quasi-polar circular orbit at 6000 km altitude. An onboard VT with quasar-like signal characteristics (Karatekin et al., 2023) will be directly observable by VGOS stations. The VT signal parameters are summarized in Table 1. SEFD values for 12 VGOS stations, derived from the analysis of log-files of one year of VGOS observations (Schartner, 2025), are listed in Table 2 for Band A.

Table 1 Genesis VT signal characteristics. Only Band–A is considered in this work.

Name	Range [MHz]	Bandwidth [MHz]
A	3100–3300	200
B	5250–5570	320
C	8200–8400	200
D	9300–9800	500

Table 2 VGOS stations and SEFD (Jy) values for Genesis Band A.

Station	SEFD	Station	SEFD	Station	SEFD
GGAO12M	2800	ISHIOKA	2500	KATH12M	4500
HOBART12	4500	KOKEE12M	3400	MACGO12M	2600
NYALE13S	1800	ONSA13NE	3400	WESTFORD	3000
WETTZ13S	3000	YARRA12M	4500	RAGEYEB	1900

Using 12 VGOS stations (Table 2), we compute the power flux density (PFD) at 1-minute intervals throughout the full day of VT transmission for Band A. This analysis is performed for multiple VT power spectral density (VT-PSD) levels and four different radiation patterns. Figure 1 illustrates the PFD as a function of elevation angle, with VT-PSD levels indicated by the colorbar. Both higher VT PSD and increased antenna directivity allow achieving the same PFD at lower elevation angles, demonstrating the advantages of focused beamforming. As VT-PSD increases, the PFD received at each station also rises proportionally. Moreover, with greater directivity, the elevation dependency becomes more pronounced; in other words, the difference between the maximum and minimum PFD received across stations increases during the simulation when directivity is considered.

However, excessively high PFD values are also not desired since the emitted signal might interfere

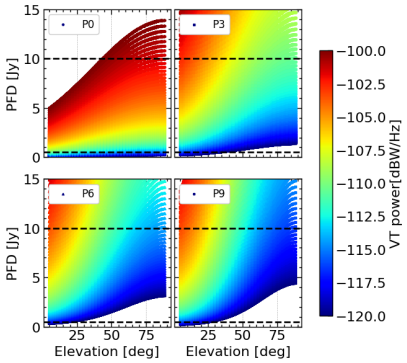

Fig. 1 PFD as a function of elevation and VT power spectral density for four different radiation patterns.

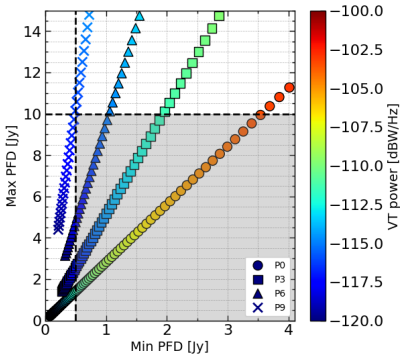

Fig. 2 Maximum and minimum PFD for all stations during the simulations for different VT power spectral density levels for each radiation pattern. The gray box confines the VT levels that deliver PFD within 0.5–10 Jy.

with observations from neighboring disciplines like astronomy. The VT-PSD and associated radiation pattern must be carefully selected to maintain PFD within an acceptable range among all stations. Figure 2 shows the minimum and maximum PFD received at the stations for each VT-PSD level, with each scatter points corresponding to the minimum and maximum values of a single curve in Figure 1. The threshold range of 0.5–10 Jy reflects discussions within the VLBI working group of ESA's Genesis Science Exploitation Team (GSET) (Haas, 2025).

The PFD levels that satisfy the threshold are confined in the gray box in Fig. 2. For the most directive antenna pattern, $P9$, none of the VT-PSD levels satisfies the desired PFD range: lower VT-PSD levels result in PFDs below 0.5 Jy at maximum distance, while higher VT-PSD levels exceed 10 Jy at minimum distance (i.e., 90° elevation). In contrast, with isotropic radiation ($P0$), the difference between minimum and maximum PFD becomes less pronounced, allowing for higher VT-PSD levels. Table 3 summarizes the maximum and minimum VT-PSD allowances for each radiation pattern (highest and lowest markers in the gray box for each radiation pattern).

Table 3 Maximum and minimum VT power spectral density values delivering PFD within 0.5–10 Jy across all VGOS stations during the simulation for each radiation pattern.

Pattern	$P_{t_{max}}$ [dBW/Hz]	$P_{t_{min}}$ [dBW/Hz]
$P0$	-104	-111
$P3$	-112	-117
$P6$	-115	-118
$P9$	-	-

Using the maximum and minimum allowable VT-PSD levels for each radiation pattern, we compute the SNR of VT observations in the Band A via Eq. 5, assuming a 10-second integration time and including all baseline combinations with elevation angles above 3°. The SEFD values of Band A for each VGOS station are listed in Table 2. Although SEFD typically varies with elevation, we assume it remains constant throughout the simulation for simplicity.

Figure 3 shows the mean SNR values for each baseline during the simulation, based on both maximum and minimum allowable power spectral density for all radiation patterns, excluding $P9$, which does not satisfy the 0.5–10 Jy PFD requirement. The corresponding $\sqrt{\mathrm{SEFD}_1 \cdot \mathrm{SEFD}_2}$ values are shown in the bottom figure for each baseline. The results highlight that SEFD is as critical as PFD in determining the SNR. For maximum allowable VT-PSD, more isotropic antenna patterns yield higher mean SNRs due to the greater permitted transmission power spectral density. At minimum VT-PSD, directive antennas provide slightly higher mean SNRs, benefiting from their focused energy distribution.

Figure 4 provides a clear overview of the mean SNR distribution across baselines. While an SNR of 20–30 is typically sufficient for VLBI quasar observations, a higher SNR improves observational sensitivity. For the lowest VT-PSD setting, approximately 50 % of the baselines achieve a mean SNR of around 25 for all radiation patterns. Under maximum VT-PSD settings, nearly all baselines exceed this threshold on average. However, realistic factors such as elevation-dependent SEFD and

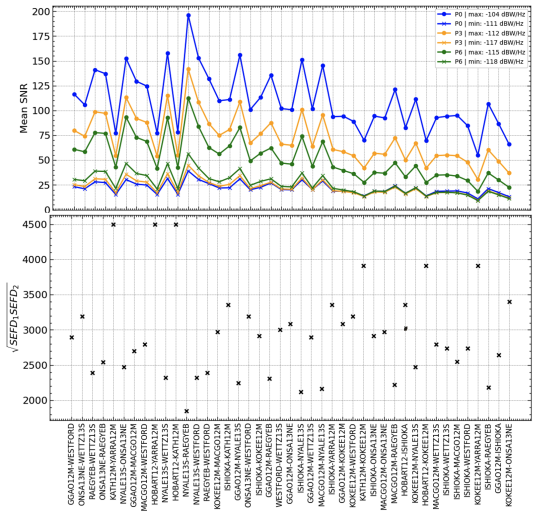

Fig. 3 Mean SNR of each baselines for Band A associated with $\sqrt{SEFD_1 SEFD_2}$ factors with 10 seconds of integration time.

atmospheric attenuation are expected to reduce the effective SNR in practice.

4 Conclusions and Outlook

In this study, we considered various VT power spectral density levels and four antenna radiation patterns onboard the Genesis satellite and computed the mean SNR across all baselines in a VGOS network during a one-day simulation for the Genesis A band. The PFD at each station was constrained to be within a 0.5–10 Jy range, and power spectral density limits were determined accordingly for each radiation pattern. This limit excluded the most directive case ($P9$) due to excessive PFD.

Using the resulting minimum and maximum allowable VT power spectral density values, we computed mean SNR values with a 10-second integration time for all baselines. Even at the lowest values, approximately 50 % of baselines achieved a mean SNR around 25 for all available radioation patterns. At maximum values, almost all baselines exceeded this threshold for all radiation patterns.

However, more realistic scenarios—including elevation-dependent SEFD and atmospheric attenuation—are expected to lower the actual SNR values. Additionally, this study assumed that the full emitted bandwidth can be observed, which might not be realistic due to technical limitations. Additionally, the study only focuses on Band A, while station sensitivity in Band D is typically reduced. Future work will incorporate these effects to refine performance estimates.

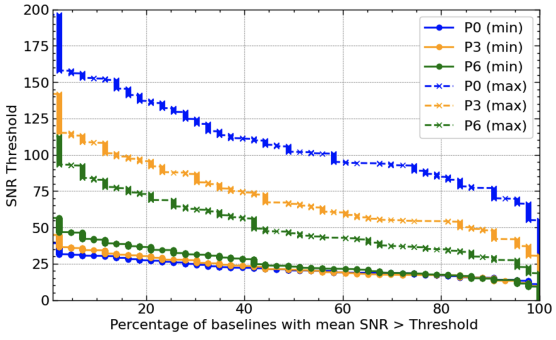

Fig. 4 Percentage of mean SNR values across all baselines exceeding a given threshold.

References

Delva P, Altamimi Z, Blazquez A, *et al.* (2023) GENESIS: co-location of geodetic techniques in space. *Earth, Planets and Space*, 75(1), 5, Springer, doi: 10.1186/s40623-022-01752-w

Haas R (2025) personal communication.

Jaradat A, Jaron F, Gruber J, Nothnagel A (2021) Considerations of VLBI transmitters on Galileo satellites. *Advances In Space Research*. (2021,5), doi: 10.1016/j.asr.2021.04.048

Karatekin Ö, Sert H, Dehant V, *et al.* (2023) VLBI signals transmitted from Earth orbiting satellites. In: *Proc.* 26th European VLBI Group for Geodesy and Astronomy Working Meeting.

Nothnagel A (2021) *Elements of geodetic and astrometric very long baseline interferometry*. TU Wien, Department of Geodesy and Geoinformation: Vienna, Austria.

Niell A, Barrett J, Burns A, *et al.* (2018) Demonstration of a Broadband Very Long Baseline Interferometer System: A New Instrument for High-Precision Space Geodesy. *Radio Science*, 53, doi: 10.1029/2018RS006617.

Schartner M, Böhm J (2019) VieSched++: a new VLBI scheduling software for geodesy and astrometry. *Publications of the Astronomical Society of the Pacific*, 131(1002), 084501, IOP Publishing, doi: 10.1088/1538-3873/ab1820.

Schartner M (2025) personal communication.

Stutzman W L, Thiele G A (2012) *Antenna theory and design*. John Wiley & Sons.

Whitney A R (1974) *Precision geodesy and astrometry via very-long-baseline interferometry*. PhD thesis, Massachusetts Institute of Technology.